STAFF SUMMARY SHEET

	TO	ACTION	SIGNATURE (Surname), GRADE AND DATE		TO	ACTION	SIGNATURE (Surname), GRADE AND DATE
1	DFP	sig	[signature], Lt Col, 26 Feb 13	6			
2	DFER	approve	Kraas, Col 26Feb13	7			
3	DFP	action		8			
4				9			
5				10			

SURNAME OF ACTION OFFICER AND GRADE	SYMBOL	PHONE	TYPIST'S INITIALS	SUSPENSE DATE
Lane, O-4	DFP	333-3615	CGC	

SUBJECT: Clearance for Material for Public Release — USAFA-DF-PA- 155

DATE: 20130220

SUMMARY

1. PURPOSE. To provide security and policy review on the document at Tab 1 prior to release to the public.

2. BACKGROUND.
Authors: Benjamin G. Ward (DFP, 719-271-6748)

Title: Modeling of transient modal instability in fiber amplfiers

Document type: Journal Article

Description: This is an article that presents a hybrid finite-element model of a fiber amplifier to study the transient behavior of the thermally induced modal instability, a common problem associated with high power fiber amplifiers.

Release Information: The paper will be submitted to Optics Express

Previous Clearance information: None

Recommended Distribution Statement: Distribution A, Approved for public release, distribution unlimited.

3. DISCUSSION. Lt. Col. Benjamin Ward is a former faculty member who continues to publish excellent research work on high performance modeling and simulation of fiber lasers and amplifiers. I am submitting this public release document on his behalf.

4. VIEWS OF OTHERS. N/A

5. RECOMMENDATION. Sign coord block above indicating document is suitable for public release. Suitability is based solely on the document being unclassified, not jeopardizing DoD interests, and accurately portraying official policy.

// signed //

CORY T. LANE, Maj, USAF
Director of Research
Department of Physics

Tab
1. Journal Article

13008 Ward

Modeling of transient modal instability in fiber amplifiers

Benjamin Ward,[1,*]

[1]*Laser and Optics Research Center, Department of Physics, United States Air Force Academy, 2354 Fairchild Drive Ste. 2A31, USAF Academy CO 8840, USA*

[*]*benjamin.ward.1@us.af.mil*

Abstract: A model of transient modal instability in fiber amplifiers is presented. This model combines an optical beam propagation method that incorporates laser gain through local solution of the rate equations and refractive index perturbations caused by the thermo-optic effect with a time-dependent thermal solver with a quantum defect heating source term. This model predicts modal instability in a 285 Watt fiber amplifier characterized by power coupling to un-seeded modes, the presence of stable and unstable regions within the fiber, and rapid intensity variations along the fiber.

OCIS codes: (140.3510) Lasers, fiber; (140.4480) Optical amplifiers; (060.5295) Nonlinear optics, fibers; (140.6810) Thermal effects.

References and links

1. Tino Eidam, Christian Wirth, Cesar Jauregui, Fabian Stutzki, Florian Jansen, Hans-Jürgen Otto, Oliver Schmidt, Thomas Schreiber, Jens Limpert, and Andreas Tünnermann, "Experimental observations of the threshold-like onset of mode instabilities in high power fiber amplifiers," Opt. Express **19**, 13218-13224 (2011) http://www.opticsinfobase.org/oe/abstract.cfm?URI=oe-19-14-13218.
2. C. Jauregui, T. Eidam, J. Limpert, and A. Tünnermann, "The impact of modal interference on the beam quality of high-power fiber amplifiers," Opt. Express **19**, 3258–3271 (2011).
3. Hans-Jürgen Otto, Fabian Stutzki, Florian Jansen, Tino Eidam, Cesar Jauregui, Jens Limpert, and Andreas Tünnermann, "Temporal dynamics of mode instabilities in high-power fiber lasers and amplifiers," Opt. Express **20**, 15710-15722 (2012) http://www.opticsinfobase.org/oe/abstract.cfm?URI=oe-20-14-15710.
4. M. Karow, H. Tünnermann, J. Neumann, D. Kracht, and P. Weßels, "Beam quality degradation of a singlefrequency Yb-doped photonic crystal fiber amplifier with low mode instability threshold power," Opt. Lett. **37**, 4242–4244 (2012).
5. Nicoletta Haarlammert, Oliver de Vries, Andreas Liem, Andrea Kliner, Thomas Peschel, Thomas Schreiber, Ramona Eberhardt, and Andreas Tünnermann, "Build up and decay of mode instability in a high power fiber amplifier," Opt. Express **20**, 13274-13283 (2012) http://www.opticsinfobase.org/oe/abstract.cfm?URI=oe-20-12-13274.
6. A. V. Smith and J. J. Smith, "Mode instability in high power fiber amplifiers," Opt. Express **19**, 10180–10192 (2011).
7. B. Ward, C. Robin, and I. Dajani, "Origin of thermal modal instabilities in large mode area fiber amplifiers," Opt. Express **20**, 11407-11422 (2012) http://www.opticsinfobase.org/oe/abstract.cfm?URI=oe-20-10-11407.
8. Cesar Jauregui, Tino Eidam, Hans-Jürgen Otto, Fabian Stutzki, Florian Jansen, Jens Limpert, and Andreas Tünnermann, "Physical origin of mode instabilities in high-power fiber laser systems," Opt. Express **20**, 12912-12925 (2012) http://www.opticsinfobase.org/oe/abstract.cfm?URI=oe-20-12-12912.
9. Kristian Rymann Hansen, Thomas Tanggaard Alkeskjold, Jes Broeng, and Jesper Lægsgaard, "Theoretical analysis of mode instability in high-power fiber amplifiers,"Opt. Express **21**, 1944-1971 (2013) http://www.opticsinfobase.org/oe/abstract.cfm?URI=oe-21-2-1944 .
10. Liang Dong, "Stimulated thermal Rayleigh scattering in optical fibers," Opt. Express **21**, 2642-2656 (2013), http://www.opticsinfobase.org/oe/abstract.cfm?URI=oe-21-3-2642 .
11. Arlee V. Smith and Jesse J. Smith, "Influence of pump and seed modulation on the mode instability thresholds of fiber amplifiers," Opt. Express **20**, 24545-24558 (2012) , http://www.opticsinfobase.org/oe/abstract.cfm?URI=oe-20-22-24545
12. Arlee V. Smith and Jesse J. Smith, "Influence of pump and seed modulation on the mode instability thresholds of fiber amplifiers," Opt. Express **20**, 24545-24558 (2012), http://www.opticsinfobase.org/oe/abstract.cfm?URI=oe-20-22-24545

13. Shakir, S.A.; Motes, R.A.; Berdine, R.W.; , "Efficient Scalar Beam Propagation Method," Quantum Electronics, IEEE Journal of , **47**, 486-491(2011), http://ieeexplore.ieee.org/xpls/abs_all.jsp?arnumber=5730173.
14. Dragic, P.D.; Ward, B.G.; , "Accurate Modeling of the Intrinsic Brillouin Linewidth via Finite-Element Analysis," Photonics Technology Letters, IEEE , **22**, 1698-1700 (2010), http://ieeexplore.ieee.org/xpls/abs_all.jsp?arnumber=5590281.
15. Satish Balay, Jed Brown, Kris Buschelman, Victor Eijkhout, William D. Gropp, Dinesh Kaushik, Matthew G. Knepley, Lois Curfman McInnes, Barry F. Smith, and Hong Zhang, *PETSc Users Manual*, (ANL-95/11 - Revision 3.3, Argonne National Laboratory, 2012), http://www.mcs.anl.gov/petsc/
16. Schermer, R.T.; Cole, J.H.; , "Improved Bend Loss Formula Verified for Optical Fiber by Simulation and Experiment," Quantum Electronics, IEEE Journal of , **43**, 899-909(2007), http://ieeexplore.ieee.org/stamp/stamp.jsp?tp=&arnumber=4300920&isnumber=4294077
17. Hadley, G.R.; , "Transparent boundary condition for the beam propagation method," Quantum Electronics, IEEE Journal of , **28**, .363-370 (1992), http://ieeexplore.ieee.org/stamp/stamp.jsp?tp=&arnumber=119536&isnumber=3419

1. Introduction

Recent evidence suggests that dynamic thermal modal instability (TMI) affects the beam quality of large mode area high average power fiber amplifiers [1,2,3,4,5]. The resulting degradation severely limits the usefulness of these devices. Efforts to improve fiber amplifier designs to mitigate this degradation benefit from numerical models that reveal the effects of amplifier parameters on performance. Several previous investigations have all but isolated the cause to refractive index gratings caused by spatial-temporal temperature variations that arise from quantum defect heating through the thermo-optic effect [6,7,8,9,10]. A key aspect of the physical description of this phenomenon is the time behavior of the temperature profile within the fiber. Under the assumption that the temperature at any point within the fiber is a periodic function of time, a steady-state solution to the optical wave equation arises that describes the process of stimulated thermal Rayleigh scattering (STRS). Numerical models have been presented that capture the essential features of STRS in fiber amplifiers [9,10,11,12]. Observations of periodic modal fluctuations in the output beams of amplifiers operating near the TMI threshold are consistent with the STRS picture of TMI [3,7]. This regime of TMI relies on the amplifier optical and temperature fields achieving a dynamic equilibrium which may be unstable with respect to external perturbation [9].

Although significant understanding is provided by the steady-state model, several factors motivate further study of the transient behavior of TMI. Amplifiers operated with a rapid turn-on may not reach steady-state equilibrium prior to the onset of TMI thus the threshold calculated using the periodic method may be higher than values that characterize realistic operating conditions. One definition of the TMI threshold has been given in terms of the buildup time required to observe the effect [5]. Also, observed TMI is often characterized by chaotic behavior [3,4,7] not able to be described in the context of a periodic model. The goal of the work presented here is to present a computational model that can enable a greater understanding of the chaotic and transient regimes of TMI. This model incorporates a 3D beam propagation method (BPM), including laser gain, for the spatial evolution of the signal field as well as a 3D time-dependent thermal model. This model is also capable of describing the steady-state periodic case.

This paper begins with a description of the BPM which is of a new type, followed by a description of the thermal solver, also of a new type. Example results are then presented and discussed.

2. Hybrid finite element-harmonic beam propagation method

The problem at hand requires the beam propagation calculation to be performed over the entire length of the fiber thousands of times, once for each time step. Each propagation step must occur over a fraction of the inter-modal beat length of the fiber leading to a requirement to evaluate upwards of one million BPM steps. Thus the computational speed of the BPM is

at a premium. Recently, a new type of BPM was presented, the azimuthal harmonic expansion beam propagation method [13], which enables much faster computation than either the split-step fast Fourier transform BPM (FFT-BPM) or finite difference BPM (FD-BPM). This method is based on a hybrid discretization in cylindrical coordinates that combines a finite-difference discretization in the radial coordinate with a harmonic Fourier expansion in the azimuthal angle. However, a 1D finite element approach in the radial direction aids treatment of fiber designs with discontinuous refractive index profiles, such as photonic crystal fibers, as well as enabling variable grid spacing to conserve the total number of unknowns in a natural fashion. A simplification of such a method has been previously applied to the study of stimulated Brillouin scattering in fibers [14].

The starting point is the scalar optical wave equation Eq. (1) valid for weakly-guiding fibers

$$\nabla^2 E(\vec{r}) + n^2(\vec{r}) k_0^2 E(\vec{r}) = 0, \tag{1}$$

where $k_0 = \omega / c$ is the free space wave-vector and $n(\vec{r})$ is the refractive index distribution. Invoking the slowly-varying envelope and paraxial approximations yields Eq. (2)

$$\left[-2i\beta \frac{\partial}{\partial z} + \nabla_t^2 + n^2(r,\varphi,z) k_0^2 - \beta^2 \right] E(r,\varphi,z) = 0 \tag{2}$$

where $E(r,\varphi,z)$ now refers to the slowly-varying envelope, β is the wave-vector describing rapid oscillations in the propagation direction, and ∇_t^2 is the transverse Laplacian operator. Setting $\partial E / \partial z = 0, \partial n / \partial z = 0$ yields an equation Eq. (3) for the stationary propagating modes of the fiber

$$\left[\nabla_t^2 + n^2(r,\varphi) k_0^2 - \beta^2 \right] E(r,\varphi) = 0. \tag{3}$$

To obtain a finite element solution of this equation the variational form Eq. (4) is introduced

$$S = \frac{1}{2} \iint_{\Omega} \left[-|\nabla_t E(r,\varphi)|^2 + n^2(r,\varphi) k_0^2 |E(r,\varphi)|^2 - \beta^2 |E(r,\varphi)|^2 \right] dA \tag{4}$$

where Ω represents the fiber cross-section. Expanding as shown in Eq. (5)

$$E(r,\varphi) = \sum_{q=-Q}^{Q} E_q(r) \exp[iq\varphi] \tag{5}$$

where Q is the truncation order of the series leads to Eq. (6)

$$\nabla_t E(r,\varphi) = \frac{\partial E}{\partial r}\hat{r} + \frac{1}{r}\frac{\partial E}{\partial \varphi}\hat{\varphi} = \sum_{q=-Q}^{Q} \left[\frac{\partial E_q}{\partial r}\hat{r} + \frac{iq}{r} E_q \hat{\varphi} \right] \exp[iq\varphi] \tag{6}$$

where Eq. (7) and Eq. (8) define the refractive index in Eq. (4),

$$n^2(r,\varphi) = n_0^2 + \sum_{q=-Q}^{Q} V_q(r) \exp[iq\varphi] \tag{7}$$

$$V_q(r) \equiv \frac{1}{2\pi} \int_0^{2\pi} \delta n^2(r,\varphi) \exp[-iq\varphi] d\varphi \tag{8}$$

where n_0 is a suitable background refractive index. With these definitions the variational form is given by Eq. (9)

$$S = -\frac{1}{2} \sum_{q=-Q}^{Q} \iint_{\Omega} \left[\left| \frac{\partial E_q}{\partial r} \right|^2 + \left(\frac{q^2}{r^2} - k_0^2 n_0^2 + \beta^2 \right) |E_q|^2 - k_0^2 \sum_{q'=-Q}^{Q} V_{q-q'} E_q^* E_{q'} \right] dA. \tag{9}$$

To accomplish the radial integral it is convenient to divide the integration domain into 1D finite elements represented by $N-1$ line segments with end points $r_k : k \in 1, N$. The integrals over the fiber cross section are then approximated as shown in Eq. (10) and Eq. (11)

$$\iint_{\Omega} f(r)\exp[iq\varphi]dA \approx \pi\delta(q)\sum_{k=1}^{N-1} f\left(\frac{r_k + r_{k+1}}{2}\right)\left(r_{k+1}^2 - r_k^2\right) \tag{10}$$

$$\iint_{\Omega} \left[f'(r)\right]^2 \exp[iq\varphi]dA \approx \pi\delta(q)\sum_{k=1}^{N-1}\left(\frac{f(r_{k+1}) - f(r_k)}{r_{k+1} - r_k}\right)^2 \left(r_{k+1}^2 - r_k^2\right) \tag{11}$$

The variational form is then conveniently expressed using matrix notation as shown in Eq. (12)

$$S = -\frac{1}{2}\mathbf{E}^* \cdot \left[\mathbf{K} - \beta^2\mathbf{M}\right] \cdot \mathbf{E} \tag{12}$$

the minimization of which leads to the generalized eigenproblem given in Eq. (13)

$$\left[\mathbf{K} - \beta^2\mathbf{M}\right] \cdot \mathbf{E} = 0 \tag{13}$$

where $\mathbf{E}$ is a vector of dimension $(2Q+1)N$ and $\mathbf{K}$ and $\mathbf{M}$ are square matrices with the same dimension. If now the envelope is allowed to vary slowly along the length of the fiber such that $\partial E / \partial z \neq 0$, then the longitudinal wave vector value k is freely chosen leading to the matrix form of the paraxial wave equation as shown in Eq. (14).

$$\left[-2ik\mathbf{M}\frac{d}{dz} + \mathbf{K} - k^2\mathbf{M}\right] \cdot \mathbf{E} = 0 \tag{14}$$

Differencing $\mathbf{E}$ with respect to z and taking one explicit and one implicit step each of distance $\Delta z / 2$ results in the usual Crank-Nicholson update rule for propagation given in Eq. (15)

$$\mathbf{E}_{m+1} = \left(\mathbf{M} + \frac{i\Delta z}{4k}\left(\mathbf{K}_{m+1} - k^2\mathbf{M}\right)\right)^{-1}\left(\mathbf{M} - \frac{i\Delta z}{4k}\left(\mathbf{K}_m - k^2\mathbf{M}\right)\right)\mathbf{E}_m \tag{15}$$

where the cumulative propagation distance is $z = (m-1)\Delta z : m \in 1, M$. In this scheme, the waveguide refractive index profile, the gain within the core, and the thermally-induced refractive index profile are incorporated as shown in Eq. (16).

$$\delta n^2(r, \varphi, z) = \delta n_{\text{wg}}^2(r, \varphi) + in_0 g(r, \varphi, z) + 2n_0 \frac{dn}{dT}\Delta T(r, \varphi, z) \tag{16}$$

where δn_{wg}^2 is the waveguiding index profile, g is the optical gain, dn / dT is the thermo-optic coefficient, and ΔT is the local temperature rise. To a good approximation, the gain is instantaneously determined by the local pump and signal intensities while the local temperature rise depends on the past history of heat deposited in the neighborhood of each point within the fiber according to the time-dependent heat equation.

The matrix $\mathbf{K}$ changes at each step due to its dependence on the signal intensity profile. To keep the gain contribution space-centered during the propagation step, the field is updated first using the initial matrix $\mathbf{K}_m$ for both the explicit and implicit steps. Then these field values are used to calculate $\mathbf{K}_{m+1}$ which is then used to repeat the implicit step. Furthermore, the average refractive index change can increase significantly over the length of the fiber

necessitating resetting the reference refractive index between steps. This is done automatically in the computer implementation.

3. Gain and heat deposition

The following discussion pertains to active media for which the atomic energy level populations are determined by two-level rate equations where instantaneous decay from the lower level to the ground state is assumed. Under these conditions the local fraction of ions in the upper state is given by Eq. (17)

$$f\left(I_s, I_p\right) = \left(\frac{I_s \sigma_{as} \tau}{h\nu_s} + \frac{I_p \sigma_{ap} \tau}{h\nu_p}\right) \Bigg/ \left(1 + \frac{I_s\left(\sigma_{as} + \sigma_{es}\right)\tau}{h\nu_s} + \frac{I_p\left(\sigma_{ap} + \sigma_{ep}\right)\tau}{h\nu_p}\right) \tag{17}$$

where $I_{s,p}$ are the signal and pump intensities, $h\nu_{s,p}$ are the energies of each signal and pump photon, σ are the absorption and emission cross-sections at the pump and signal wavelengths, and τ is the upper-state lifetimes. The gain is then given by Eq. (18)

$$g\left(r,\varphi,z\right) = N_{\text{ion}}\left[f\left(r,\varphi,z\right)\sigma_{es} - \left(1 - f\left(r,\varphi,z\right)\sigma_{as}\right)\right] \tag{18}$$

where N_{ion} is the doping density. Similarly, the pump gain is given by Eq. (19)

$$g_p\left(r,\varphi,z\right) = N_{\text{ion}}\left[f\left(r,\varphi,z\right)\sigma_{ep} - \left(1 - f\left(r,\varphi,z\right)\sigma_{ap}\right)\right]. \tag{19}$$

For cladding-pumped amplifiers, the paraxial approximation is generally not valid for the pump light guided in the cladding due to its large numerical aperture. Therefore, constant pump intensity throughout the cladding is assumed to be maintained through the process of mode mixing so that the evolution of the pump intensity is given by Eq. (20)

$$\frac{d}{dz} I_p\left(z\right) = \pm \frac{1}{A_{\text{clad}}} \iint_{\Omega} g_p\left(r,\varphi,z\right) I_p\left(r,\varphi,z\right) dA \tag{20}$$

where A_{clad} is the area of the pump cladding and the $\pm$ represents counter versus co-pumping arrangements. The heat load due to the quantum defect is then given by the number of ions going through the cycle multiplied by the rate that they go through the cycle and the quantum defect for each photon as shown in Eq. (21)

$$Q(r,\varphi,z) = N_{\text{ion}}\left(\frac{\nu_p}{\nu_s} - 1\right) f(r,\varphi,z)\sigma_{es} I_s(r,\varphi,z) \tag{21}$$

The normalization of the optical fields is chosen so that $I_s = |E|^2$. Starting from some known temperature distribution, the temperature evolves in time at each spatial point according to the time-dependent heat equation given by Eq. (22)

$$\frac{\partial}{\partial t} T\left(r,\varphi,z,t\right) = \frac{K}{\rho C} \nabla^2 T\left(r,\varphi,z,t\right) + \frac{1}{\rho C} Q\left(r,\varphi,z,t\right) \tag{22}$$

where K is the thermal conductivity, ρ is the mass density, and C is the heat capacity within the fiber. This equation is amenable to a solution approach similar to that used for the optical propagation equation. Both T and Q are approximated in r and φ using the 1D finite element scheme in the radial direction and the azimuthal harmonic expansion. The longitudinal component of the Laplacian is evaluated using finite differences in the temperature values at the z points defining the optical beam propagation steps as shown in Eq. (23)

$$\left.\frac{\partial^2}{\partial z^2}T(r,\varphi,z)\right|_m \approx \frac{1}{\Delta z^2}\left[T_{m+1}(r,\varphi)-2T_m(r,\varphi)+T_{m-1}(r,\varphi)\right] \tag{23}$$

To a good approximation, the thermal properties of the fiber are constant throughout the cross-section. Significantly, this causes the different azimuthal harmonic terms to de-couple yielding $(2Q+1)$ independent Crank-Nicholson time step update equations for the temperature distribution as shown in Eq. (24)

$$\mathbf{T}_{q,l+1} = \left[\mathbf{M}_{\mathrm{TH}} + \frac{\Delta t}{2}\frac{K}{\rho C}\mathbf{K}_{q,\mathrm{TH}}\right]^{-1}\cdot\left[\left(\mathbf{M}_{\mathrm{TH}} - \frac{\Delta t}{2}\frac{K}{\rho C}\mathbf{K}_{q,\mathrm{TH}}\right)\cdot\mathbf{T}_{q,l} + \frac{\Delta t}{2\rho C}\mathbf{M}_{\mathrm{TH}}\cdot\left(\mathbf{Q}_{q,l+1}+\mathbf{Q}_{q,l}\right)\right] \tag{24}$$

where l is the time step index, Δt is the time step, q is the harmonic component, $\mathbf{T}_{q,l}$ are vectors of length $M\cdot N$ and $\mathbf{M}_{\mathrm{TH}}, \mathbf{K}_{q,\mathrm{TH}}$ are sparse matrices of this same dimension. These sparse matrices are assembled by inserting blocks of values that when multiplied by the $\mathbf{T}_{q,l}$ approximate the integrals over the fiber cross-section as described by Eq. (25) and Eq. (26):

$$\mathbf{M}_{\mathrm{TH}} = \sum_{k=1}^{N-1}\sum_{m=1}^{M}\Delta A_k\left[\mathbf{v}_{k,m}\cdot\mathbf{v}_{k,m}^{\mathrm{T}}\right] \tag{25}$$

$$\begin{aligned}\mathbf{K}_{q,\mathrm{TH}} = -\sum_{k=1}^{N-1}\sum_{m=1}^{M}\Delta A_k\Bigg[&\frac{1}{\Delta r_k^2}\mathbf{u}_{k,m}\cdot\mathbf{u}_{k,m}^{\mathrm{T}} + \frac{4q^2}{\left(r_k+r_{k+1}\right)^2}\mathbf{v}_{k,m}\cdot\mathbf{v}_{k,m}^{\mathrm{T}}\\ &+\frac{1}{\Delta z^2}\left(\mathbf{v}_{k,m+1}\cdot\mathbf{v}_{k,m+1}^{\mathrm{T}} - 2\mathbf{v}_{k,m}\cdot\mathbf{v}_{k,m}^{\mathrm{T}} + \mathbf{v}_{k,m-1}\cdot\mathbf{v}_{k,m-1}^{\mathrm{T}}\right)\Bigg]\end{aligned} \tag{26}$$

where ΔA_k is the area of the annulus with inner and outer radii of r_k and r_{k+1}, $\mathbf{v}_{k,m}$ are column vectors that have two non-zero entries each with value $1/2$ at locations $m\cdot N+k$ and $m\cdot N+k+1$, and $\mathbf{u}_{k,m}$ are column vectors that have two non-zero entries with values -1 and 1 at locations $m\cdot N+k$ and $m\cdot N+k+1$. The choice to order the vectors $\mathbf{T}_{q,l}$ first in k is arbitrary and leads to contiguous blocks non-zero entries of dimension N in the matrices.

To keep the time step update centered in time, the harmonic components of the heat load given by Eq. (27)

$$\mathbf{Q}_{q,lzm} = \frac{1}{2\pi}\int_0^{2\pi} Q(r_k,\varphi,z_m,t_l)\exp\left[-iq\varphi\right]d\varphi \tag{27}$$

must be evaluated at the beginning and end of each time step. Therefore the updated temperature is calculated first using the initial heat distribution. This temperature distribution is then used to update the optical field leading to the updated heat distribution. This is then used to repeat the temperature update, this time incorporating the heat distributions at the beginning and end of the time step. To start the simulation an initial temperature distribution, input mode field, and input pump power must be specified.

The input mode field is taken to be a superposition of guided modes with pre-specified amplitudes. Additionally, a time-dependent phase shift may be applied to one or more of the input modes to incorporate a frequency shift between modes as shown in Eq. (28)

$$E(r,\varphi,0,t) = \sum_{n=1}^{N}\sqrt{P_n}E_n(r,\varphi)\exp\left[if_n(t)\right] \tag{28}$$

where P_n and $E_n(r,\varphi)$ are the power and mode field distribution of guided mode n. This has been shown to induce inter-modal coupling through the process of stimulated thermal Rayleigh scattering [9,10,11,12].

4. Computational implementation

The model described above is a 3+1D fiber amplifier model with a hybrid discretization scheme in cylindrical coordinates employing finite elements in the radial direction, a harmonic expansion in the azimuthal direction, and a finite difference grid in the direction of optical propagation. For a fiber length of 1.63 meters with a beat length of 22.3 millimeters, 100 samples per beat length lead to a longitudinal grid with 7300 points. The finite element approach in the radial dimension permits variable radial point spacing thus reducing the number of radial points to about 100 that span the entire fiber cladding radius, resulting in a matrix order of approximately 7.3×10^5 for each of the $(2Q+1)$ thermal matrices. Since the region involved in optical propagation is only at the center of the fiber, a subset of the thermal radial points is used in the optical propagation equations. This region is typically 2~3 times the core size. Fig. 1 depicts the computational steps required to implement this method.

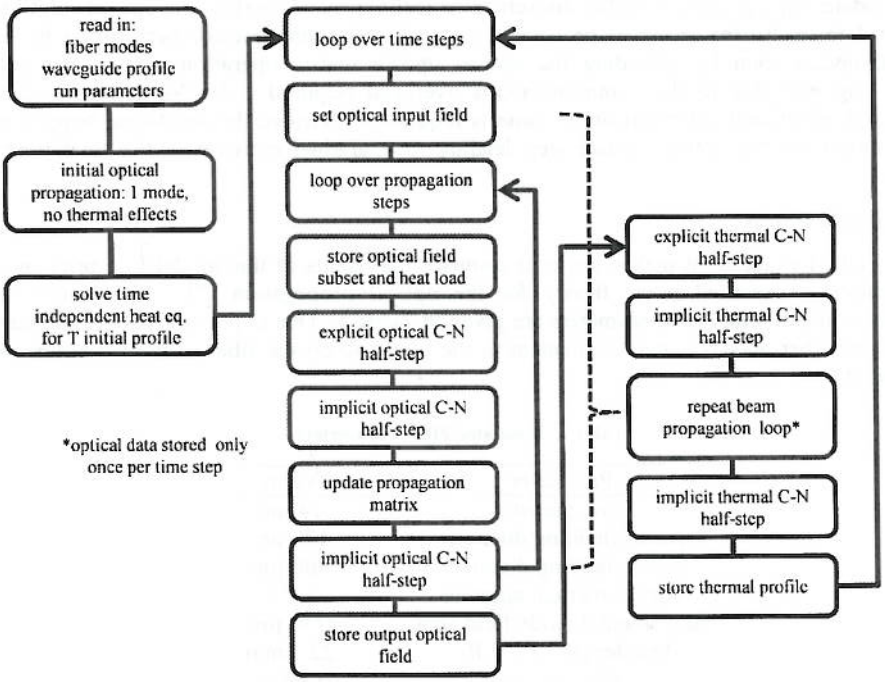

Fig. 1. Sequence of required to carry out the time dependent amplifier simulation.

This approach can be used for any waveguide profile for which the harmonic expansion can be calculated, however, those with stronger azimuthal variations require higher truncation orders. It is convenient to use separate truncation orders Q for the optical and thermal problems. For modeling photonic crystal fibers with small capillaries truncation orders of $Q_{opt} \approx 10-20$ are appropriate while for step index fibers, Q_{opt} can be chosen to include the highest azimuthal order propagating modes supported by the fiber. For typical large mode area fibers $Q_{opt} \approx 2-4$ suffices. Likewise, the averaging effect resulting from heat diffusion

means that $Q_{therm} \square 2-4$ for all types of fibers. Nevertheless, the orders may be increased until the desired level of convergence is achieved. The simulation time is most sensitive to Q_{opt} because this affects the speed of the beam propagation portion of the calculation which is the most time consuming. The simulation time of a large pitch photonic crystal fiber was observed to be about five times greater than that of a step index fiber.

Within this approach, the primary computational tasks are sparse matrix multiplication and sparse linear system solution. Various software packages are available for these tasks that take advantage of modern multi-processor high performance computing architectures. The implementation reported here relies on parallelization using the message passing interface (MPI) [15]. Within MPI, each collective task on the processor grid is mediated through an MPI communicator. To solve all harmonic components of the thermal problem simultaneously, the processor grid is divided into sub-communicators, one for each harmonic component. Therefore, as long as processors are available, the thermal harmonic order may be increased with negligible increase in the time required to accomplish the thermal update.

During the beam propagation portion of the calculation, the temperature distribution remains stationary in memory scattered across the processing grid and the required temperature values are broadcast to all processes at each spatial propagation step. The hybrid discretization scheme greatly reduces the number of floating point operations required for each update step compared to other discretization techniques. Therefore the optical solution is obtained faster by the group of processors on each sub-communicator performing its own optical update than by spreading the optical update matrix operations across the entire processing grid due to the communications overhead required. As the thermal order is increased, additional communications time is required to retrieve the additional temperature information for the optical update step leading to a gradual increase in the total time to solution.

5. Example results

As a first example, it makes sense to compare the results of this model to a prior model that employed coupled mode theory for the optical propagation [7]. The double-clad Ytterbium-doped amplifier parameters are given in Table 1. Due to the calculation speedup, a step index fiber approximately equivalent to the photonic crystal fiber discussed before was simulated.

Table 1. Simulated Fiber Parameters

Parameter	Value
core diameter	74 μm
pump cladding diameter	170 μm
outer cladding diameter	400 μm
core numerical aperture	0.03
fundamental mode field area	2750 μm^2
beat length LP_{01}-LP_{11}	22.3 mm
fiber length	1.63 m
yb^{+3} doping concentration	3.5×10^{25} m^{-3}
signal wavelength	1.064 μm
pump wavelength	0.977 μm
signal power LP_{01}	9.5 W
signal power LP_{11}	0.5 W
pump power	357 W
signal emission cross-section	3.58×10^{-25} m^2
signal absorption cross-section	6.00×10^{-27} m^2
pump emission cross-section	1.87×10^{-24} m^2
pump absorption cross-section	1.53×10^{-24} m^2

upper state lifetime	850 μs
thermal conductivity	1.38 W/m-K
heat capacity	703 J/kg-K
mass density	2200 kg/m^3
thermo-optic coefficient	1.2×10^{-5} K^{-1}
heat sink temperature	300 K
z grid spacing	2.23×10^{-4} m
time step	1.0×10^{-5} s
total simulation time	10 ms
thermal radial points	101
optical radial points	56
doped core radial points	30
optical azimuthal order	3
thermal azimuthal order	2

Furthermore, there was no material, scattering, or bend loss assumed. The outer boundary of the fiber cladding is maintained at a fixed reference temperature thus assuming perfect conductive cooling. Also, the pump and signal linewidths were assumed negligible.

A counter-pumped configuration was assumed for this simulation in which the total pump absorption throughout the fiber was approximated to be constant so that the pump intensity at the seeded end could be set as a boundary condition.

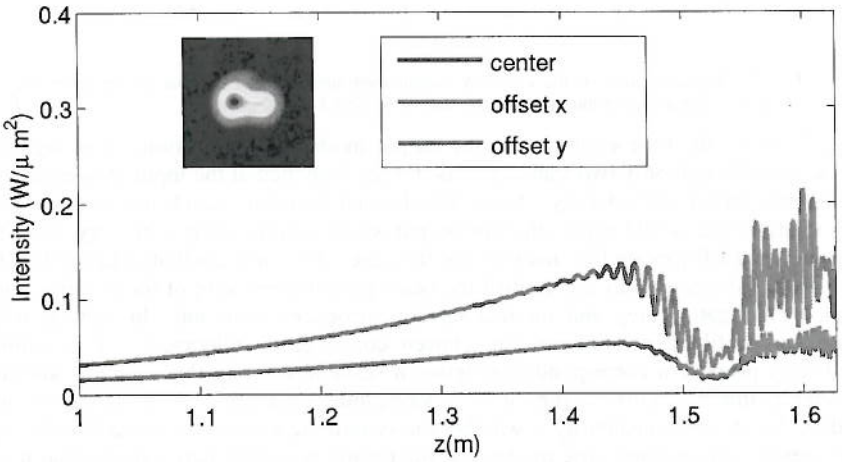

Fig. 2. Plot of the optical intensity as a function of length at the center of the fiber core and at points offset from the center of the fiber core by half the core radius after a simulation time of 10 ms. The accompanying movie (Media 1) shows the evolution of these intensity probes over a time period of 10 ms. The inset shows the optical field at the output.

Fig. 2 and the accompanying movie show the time dependence of the optical intensity within the fiber core and the output intensity distribution over time. The simulation was started with all of the power launched into the LP_{01} mode and then the LP_{11} was gradually introduced over a period of 0.1 ms. The introduction of the higher order mode immediately causes the output to become unstable. In agreement with the coupled mode theory results [7] the instability is confined to the latter portion of the amplifier and is more severe near the output end. Furthermore, as time progresses the stable region grows in extent as the thermally induced grating reaches stable equilibrium. This equilibrium region is possible due to the fact that the two modes are launched at the same optical frequency and so no moving grating exists at the seed end [6]. This is also in agreement with the coupled mode theory results [7].

While there are some similarities between the appearances of Fig. 1 and Fig. 2 of [7] different quantities are being plotted. Fig. 1 shows the local intensity probe at three points

while the prior published figure shows the modal content. The full optical field that is required to calculate the modal content was not stored at every longitudinal position for every time step due to the large file size that would be required. Nevertheless, rapid spatial oscillations characteristic of non-adiabatic power transfer [8] are evident in both. The beam propagation model described here also captures the effect of thermal lensing on the mode field area of the fundamental mode of the fiber. The mode field area of the cold fiber is 2750 μm^2 and at the output end of the heated fiber, the area decreased to 1960 μm^2.

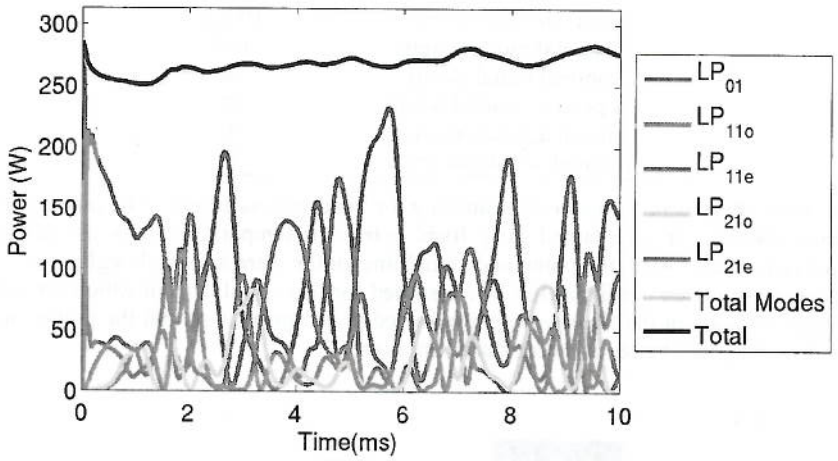

Fig. 3. Modal content of the amplifier output over time as well as total power from the integrated optical output intensity and the sum of the first 8 modal powers.

Fig. 3 shows the time evolution of the output modal decomposition. It is significant to note that even though only two transverse modes are launched at the input, power scatters into other modes almost immediately. Since the thermal boundary condition was symmetric in this simulation, one would expect that the output would retain mirror symmetry about the axis of the launched LP_{11} mode but this was not the case. This was attributed to the fact that the sparse linear solvers used to accomplish the beam propagation were of the iterative variety so that each propagation step and thermal update introduces error into the optical fields and temperature profile depending on the chosen convergence tolerance. It is tempting to immediately propose a correspondence between residual error in the equation solutions and unavoidable imperfections in the optical waveguide structure. A fundamental question regarding the observed instability is whether the symmetric solution is unstable with respect to power present in non-symmetric modes and the results presented here suggest that it is. This matter warrants further study that is beyond the scope of this paper.

The total output power was found to fluctuate in disagreement with some reports [4]. This is attributable to the fact that the spatial fluctuations of intensity within the fiber inhibit efficient extraction of the available gain thus causing the uniform pump absorption approximation to break down. This observation suggests an additional mechanism for feedback that can drive the instability. It has been shown that amplitude fluctuations at the seeded end of amplifiers can cause a steady-state amplifier solution to become unstable [9]. If fluctuations in the spatial intensity cause varying amounts of pump to be absorbed in a counter-pumped configuration, this would effectively modulate the seed level present near the input end of the amplifier thus providing the feedback mechanism modulating the amplitude causing instability.

It is also apparent that the incorporation of the beam propagation model significantly lowers the instability threshold. The pump power of 357 W in the simulation here was below the previously observed approximate instability threshold of 1060 W [7] for the conductively-cooled case and yet instability is clearly present. This suggests that models of the transient

regime based on coupled mode theory should include all guided modes in order to accurately capture instability behavior. This also agrees with the observation that larger cores that support more transverse modes exhibit lower instability threshold powers. Experimentally-observed instability thresholds for this type of amplifier are yet lower so clearly the incorporation of the beam propagation model improves prospects for agreement of the model with observed thresholds.

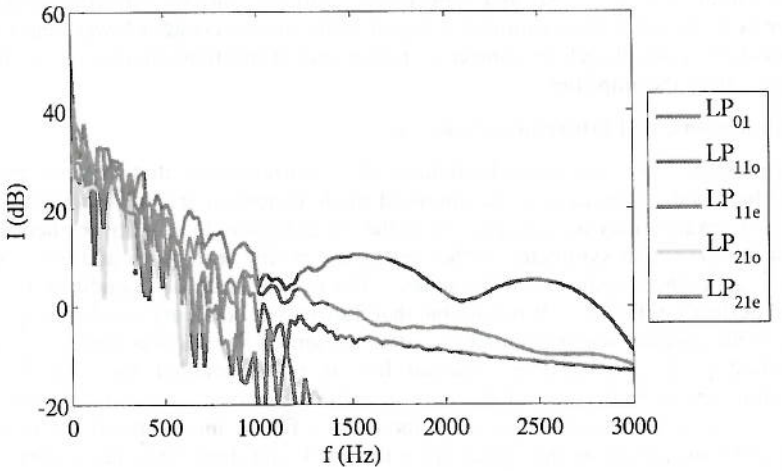

Fig. 4. Frequency spectra of the first five modes of the simulated fiber.

Fig. 4. shows the frequency spectra of the transverse modes at the fiber output. No sharp frequency peaks are visible indicating a degree of randomness in the output. Also, the high frequency tail was more prominent in the lower-order modes, which is not immediately evident just by examining the time series shown in Fig. 3.

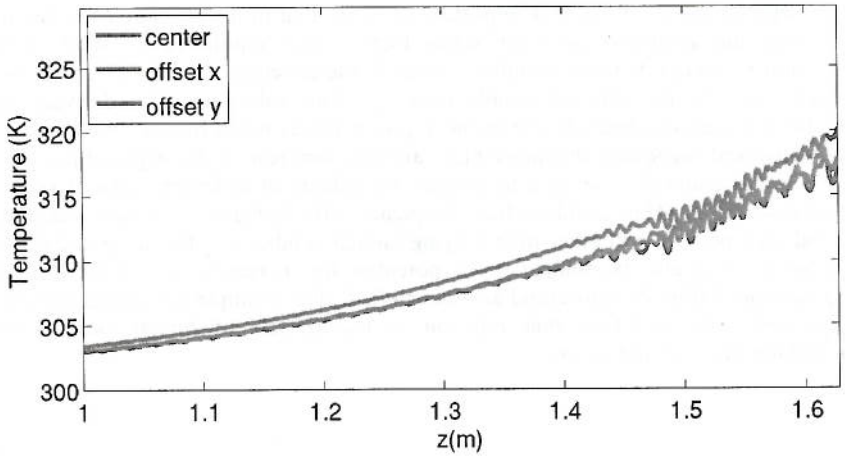

Fig. 5. Temperature distribution as a function of length at the fiber core and at points offset from the center of the fiber core by half the core radius. The accompanying movie (Media 2) shows the evolution of these temperature probes over a time period of 10 ms.

The temperature was recorded in time at the same sampling points as the optical intensity throughout the fiber and is presented in Fig. 5. As expected, the temperature is static in the region of the fiber not experiencing instability but is irregular where the optical intensity fluctuates. Due to the length of the thermal diffusion time, the temperature cannot keep up

with the rapidly fluctuating intensity. Rather, it exhibits slowly varying behavior that captures a windowed time average of the quantum defect heating profile. Both the center temperature and the amplitude of the temperature fluctuations are irregular and not uniform across the core as revealed by the difference between the profiles at the core center and off center. Observing the time evolution of the temperature profile from the beginning of the simulation where all of the power was in the LP_{01} mode reveals an immediate overall temperature drop as power is first introduced into the LP_{11} mode and then coupled into the other higher order modes. This is consistent with the prior observation that higher order modes create a lower heat load than the fundamental [7] and therefore transfer of power out of the fundamental mode decreases the optical length of the amplifier.

6. Model limitations, and future investigations

The model presented here has some limitations in its current form that deserve discussion. The first is that bending losses and bend-induced mode distortion are not accounted for. An effective index gradient may be incorporated in the usual fashion to account for bending [16]. This breaks the azimuthal symmetry of the step-index profile leading to additional terms in the harmonic azimuthal expansion of the index. The optical boundary condition use here is lossless and perfectly reflecting. It is possible that transparent boundary conditions [17] could be adapted to the paraxial scalar beam propagation presented here as was done for a previous similar method [13]. Furthermore, material loss is not accounted for. In the current implementation, the doped region of the core must be assumed to be uniform and circular. While this is true of some step index large mode area fibers, micro-structured fibers often have some additional structure that arises from the stack and draw fiber fabrication method. As was already mentioned above, the presented model does not hold the launched pump perfectly constant for counter-pumped configurations which are practically a necessity for minimizing the effective amplifier length to maximize non-linear thresholds. An efficient method for overcoming this limitation in the transient regime is not immediately apparent. Finally, in its current form, this model requires high-performance computing resources to use. It is not suitable for desktop computers.

The model presented here can enable numerous future investigations a few of which are briefly discussed below. First, it is important to verify that in the absence of noise, quantum or otherwise, the amplifier can reach stable thermo-optic equilibrium. While a previous investigation predicted dynamic instability even in the absence of such noise [7], this could have been due to limits in the achievable accuracy of the solutions of the derived equations. This instability was also predicted to occur at power levels much higher than those at which has been observed suggesting that noise plays an important role in the origin of instability.

This model could also be used to analyze the effects of different types of noise on the onset of instability. This could include frequency offsets between modes, fluctuations of pump and seed powers, and other time varying launch conditions. Build up and decay times of instability could also be studied. The potential for increasing the instability threshold through advanced fiber designs could also be studied. For example the model can treat large pitch photonic crystal fibers that rely on de-localization of higher order modes for fundamental mode discrimination.

7. Conclusion

A model of transient modal instability in fiber amplifiers has been presented. This model relies on a time-dependent 3-dimensional treatment of the effects of quantum defect heating on the waveguiding properties of amplifier fibers. This model has confirmed some predictions first made using coupled-mode theory. These include the existence of stable and unstable regions along the length of the fiber, their evolution over time, the increase in the severity of the instability toward the output end of the fiber, and rapid optical intensity variations along the fiber. It has also exhibited several additional aspects of TMI including coupling to un-seeded modes and lower onset threshold powers compared to a prior model that are more in line with experimental observations.

Efforts have been made to reduce the time required to perform the calculations including the realization of a new hybrid finite element, harmonic beam propagation method, a hybrid finite element, harmonic, finite difference thermal solver, and parallel implementation on modern high performance computing architectures using the message passing interface. This method should prove a useful tool in studying and eventually overcoming the technological challenges presented by TMI in high average power fiber amplifiers.

Acknowledgments

This work was made possible by a grant of computing time at the U S. Army Engineer Research and Development Center Department of Defense Supercomputing Resource Center from the U. S. Department of Defense High Performance Computing Modernization Program. The author would like to thank R. Andrew Motes for helpful discussions. Distribution A: Approved for public release. Distribution unlimited.